Optical Materials 144 (2023) 114325

Contents lists available at ScienceDirect

Optical Materials

journal homepage: www.elsevier.com/locate/optmat

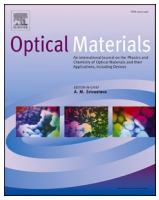

Research Article

Synergizing tin dioxide/perovskite interface with fluorine-doped zinc oxide for stabilized and efficient carbon-based perovskite solar cells

Anupam Yadav [a], M.I. Sayyed [b,c], Nafis Ahmad [d,*], S. Kevin Vargas-Portugal [e], A.M. Alshehri [d], Anmar Ghanim Taki [f], Russul thabit [g], Ayat Hussein Adhab [h]

[a] Department of CEA, GLA University, Mathura, 281406, India
[b] Department of Physics, Faculty of Science, Isra University, Amman, 11622, Jordan
[c] Department of Nuclear Medicine Research, Institute for Research and Medical Consultations (IRMC), Imam Abdulrahman Bin Faisal University, P. O. Box 1982, Dammam, 31441, Saudi Arabia
[d] Department of Physics, College of Science, King Khalid University, P.O. Box: 960, Abha, 61421, Kingdom of Saudi Arabia
[e] Department of Civil Engineering, Faculty of Engineering, Universidad Tecnológica de los Andes, Peru
[f] Department of Radiology & Sonar Techniques, Al-Noor University College, Nineveh, Iraq
[g] Pharmacy College, Al-Farahidi University, Iraq
[h] Department of Pharmacy, Al-Zahrawi University College, Karbala, Iraq

ARTICLE INFO

Keywords:
Electron transport layer
Carbon electrode
Perovskite solar cells
Interface engineering
Tin dioxide

ABSTRACT

The new generation of solar cell technology, perovskite solar cells (PSCs), are the most promising candidates to meet global energy demands. In the current study, we improved the efficiency of their cost-effective type, i.e., carbon-based PSCs, by employing an interface engineering on the tin dioxide (SnO_2) electron transport layer (ETL). A fluorine doped-zinc oxide material was used to treat the SnO_2 layer and prepare a better substrate for perovskite fabrication. The fabricated perovskite layer on the treated SnO_2 reveals better charge transfer, lower charge recombination, and lower leakage current. In addition, the fabricated perovskite layer on the modified ETL showed improved crystalline properties with passivated grain boundaries. As a result, a champion efficiency of 15.22% was recorded for the target carbon-based PSCs, referring to improved photovoltaic performance. Notably, the target devices showed a higher stability behavior against ambient air and kept 95% of their initial efficiency after 1658 h ageing time.

1. Introduction

New generation solar cell technology, i.e., perovskite solar cells (PSCs), is the most favored research area to solve global energy demands for green energy [1–4]. Excellent optoelectrical properties of perovskite materials, including intense light absorbing ability, long-term carrier lifetimes, tunable bandgap, and defects tolerance, tailor these materials for solar cell application [5–8]. For the first time, Miyasaka et al. developed $MAPbI_3$ perovskite as a light-harvesting layer for solar cells and recorded an efficiency of 3.8% [9,10]. After 15 years, the efficiency of PSCs rose to certified 25.5% [11].

State-of-the-art efficient PSCs usually employ expensive hole transport layers (HTLs) and metal electrodes, which increase prime cost and reduce the environmental stability of this technology. Spiro-OMeTAD material is one of the most used HTLs in PSCs. To improve the hole mobility of this material, researchers usually doped it with lithium bis (trifluoromethylsulfonyl)imide (LiTFSI), 4-(*tert*-butyl)pyridine (*t*BP), and Tris[2-(1H-pyrazol-1-yl)-4-*tert*-butylpyridine]-cobalt(III)-tris[bis-(trifluoromethylsulfonyl)imide] (FK209) [12–14]. These dopants induce degradation processes of HTL and perovskite layer by exposing PSCs to heating, humidity, and irradiance [15–17]. In contrast, HTL-free PSCs with carbon electrodes offer us stable and cost-effective solar cells [18–21]. HTL-free carbon-based PSCs suffer from low efficiency, and further attempts need to address this issue and record considerable efficiency.

Chen et al. employed a solvent engineering method in a two-step sequential $MAPbI_3$ fabrication. Indeed, they dissolved MAI salt into a mixed isopropanol/cyclohexane solvent. They concluded that this mixed solvent induces the conversion of PbI_2 to $MAPbI_3$ and suppresses the ostwald ripening process, recording a champion efficiency of

* Corresponding author.
E-mail address: nafis.jmi@gmail.com (N. Ahmad).

https://doi.org/10.1016/j.optmat.2023.114325
Received 14 July 2023; Received in revised form 23 August 2023; Accepted 31 August 2023
Available online 5 September 2023

14.38% for carbon-based HTL-free PSCs [22]. Zhou et al. added tungsten oxide nanoparticles (NPs) as an additive to the carbon electrode to promote hole extraction at the perovskite/carbon interface. They recorded a champion efficiency of 10.77% [23]. Omrani et al., by simulation, showed that using NPs as interface modifiers, and thanks to local surface plasmon resonance phenomena, could reach a PCE of 19.72% for carbon-based HTL-free PSCs [24]. They believed that plasmonic NPs generate hot electrons during plasmon resonance, which can be directly injected into their surrounding perovskite environment and increase photo-generated electrons mobility by filling the trap states. Modifying the SnO_2/perovskite interface with SnO_2 QDs is another way to improve the efficiency of carbon-based HTL-free PSCs. SnO_2 QDs interfacial layer induces the carriers extraction, increasing the performance of the fabricated devices to 11.7% [25]. Cadmium halides, including $CdCl_2$, $CdBr_2$, and CdI_2, are good candidates to improve the performance of carbon-based HTL-free PSCs. Qiu et al. employed these materials to modify the SnO_2 and obtained a champion efficiency of 14.47%. They concluded that Cd^{2+} ions passivate the bulk and surface SnO_2 defects, improving the transfer of electron carriers and blocking holes [26]. Shi et al. introduced the cetyltrimethylammonium bromide (CTABr) to modify the perovskite/carbon interface. They recorded a PCE of 11.26% thanks to the energy level alignment caused by CTABr material [27]. Recently, Zhong et al. used ammonium acetate (NH_4Ac) as an additive for the anti-solvent engineering method and recorded an efficiency of 15.43%. They declared that the NH_4Ac adjusts the nucleation density and retards the perovskite crystallization. The NH_4Ac assists in producing dense and pinhole-free perovskite films, enlarging grains, and passivating grain boundaries [28].

Here, we focused on improving the efficiency and stability of carbon-based HTL-free PSCs by modification of SnO_2 ETL/perovskite with fluorine-doped zinc oxide (F–ZnO) NPs. We dissolved F–ZnO NPs in ethanol with different concentrations and spin-coated on the pre-formed SnO_2. It was observed that modification of SnO_2 with the desired F–ZnO solution facilitates electron extraction to ETL, reducing charge recombination losses within solar cells. In addition, the treated SnO_2 prepares a suitable substrate for the deposition of a perovskite layer, which leads to forming a perovskite layer with reduced surface defects and passivated grain boundaries. The F–ZnO-based interface engineering record us a champion efficiency of 15.22% with boosted environmental stability behavior.

1.1. Experimental details

1.1.1. Synthesis of fluorine doped-zinc oxide

Fluorine-doped zinc oxide (F–ZnO) was synthesized by dissolving 59.5 g of $Zn(NO_3)_2{\cdot}6H_2O$ (Merck, 98%) in 200 mL of ethanol (EtOH, Merck, 99.8%). Next, three mol% NH_4F (Merck, 98%) was dropwise added into the above solution. The obtained solution was stirred for 120 min at 65 °C. Then, the ammonium hydroxide (NH_4OH, Merck, 25%) solution was dropwise added into the above solution to reach a PH of 9 while continuously stirring to generate white colloids. The obtained colloids were filtered and washed with DI water to reduce PH to 7. The obtained powder was heated at 60 °C in an oven for 24 h for drying. Finally, the dried powder was calcined at 500 °C for 2 h to obtain F–ZnO NPs.

1.1.2. Device preparation

$SnCl_2.2H_2O$ (98%, Merck) solution (66 mM) in EtOH is deposited over the cleaned FTO by spin-coating at 3000 rpm for 45 s to obtain SnO_2 ETLs. The SnO_2 ETLs were annealed, first at 100 °C for 10 min and then at 190 °C for 60 min. After that, F–ZnO NPs are dissolved in EtOH with concentrations of 0.0–9.0% and spin-coated over the SnO_2 layers. This step is done to modify SnO_2/Perovskite interface. Here $MAPbI_3$ was used as a light-harvesting perovskite layer. Its pre-solution was prepared by dissolving 0.461 g of lead iodide (PbI_2, 99.9%, Lumtec) in 700 μL of mixed solvents of dimethyl sulfoxide (DMSO, 99.9%, Merck) and dimethylformamide (DMF, 99.8%, Merck) in a volume ratio of 1:9, followed by stirring at 80 °C for 45 min. Then, 0.159 g of methylammonium iodide (MAI, 99.8%, Lumtec) was mixed with the PbI_2 precursor and shacked for 3 min at RT. The perovskite layer was formed by spin coating 75 μL of $MAPbI_3$ solution over the ETLs at 4000 rpm for 30 s. Then, they are annealed at 98 °C for 20 min. During the spin coating process, 500 μL of toluene (99.8%, Merck) was swiftly poured on perovskite to promote perovskite growth. Dyenamo, DN–CP01 carbon paste was bladed on the $MAPbI_3$ films to fabricate carbon electrodes, followed by annealing at 70 °C for 30 min.

1.1.3. Characterization

A TEM Philips EM 208S and Mira3, TESCAN field emission SEM instruments were employed to record TEM and FESEM images of samples, respectively. An XRD Philips PW1730 X-ray diffractometer collected the XRD patterns of F–ZnO NPs and perovskite layers. A UV-VIS Thermo Biomate5 spectrophotometer investigated the absorbance of F–ZnO NPs and perovskite films. A PL CARY ECLIPSE device recorded the photoluminescence (PL) response of different perovskite layers. To measure PL, samples were excited at a wavelength of 450 nm. A Keithley 2401 source, under a calibrated AM 1.5 light irradiance, measured current density-voltage curves of carbon-based HTL-free PSCs to calculate the photovoltaic performance and stability behavior of devices. A contact angle CAG-20 instrument was used to calculate the contact angle of water droplets on perovskite layers.

2. Results

Fig. 1a and b show the FE-SEM and TEM images of the synthesized F–ZnO NPs, respectively. As can be seen, F–ZnO NPs show a spherical grain morphology with a size range of 25–50 nm. Fig. 1c shows the UV–Vis spectra of F–ZnO NPs. The F–ZnO NPs reveal a characteristic peak at 375 nm, which refers to the successful synthesis of ZnO NPs [29]. Finally, Fig. 1d shows the XRD pattern of the F–ZnO NPs. The XRD pattern shows four prominent peaks at 31.8°, 34.4°, 36.3°, and 47.5° referring to planes (100), (002), (101), and (102). These peaks prove the successful formation of F–ZnO NPs [30].

The results of perovskite films' UV–Vis absorption (Fig. 2a) were depicted in Fig. 2a. Notably, the perovskite layer created on SnO_2 treated with 6% F–ZnO solution exhibits a greater absorption along the visible area due to the improved crystallinity and better micromorphology. The treated SnO_2/Perovskite interface does not affect the perovskite film's energy bandgap, and all layers show the same absorption edge wavelength. The steady-state photoluminescence (PL) spectra of the deposited films are displayed in Fig. 2b. The films' typical emission peak, which is at 784 nm, agrees with the UV–Vis spectra. According to Fig. 2b, with the increase of F–ZnO concentration up to 6%, the intensity of the PL decreases. In the concentration of 9%, the PL intensity has increased compared to the concentration of 6%. The perovskite/SnO_2+F–ZnO 6% exhibits the highest PL quenching efficiency, indicating improved electron extraction capabilities due to interface engineering caused by the F–ZnO solution. These results indicate that the SnO_2+6% F–ZnO film contributed to reducing charge recombination centers by improving the thin film quality of the $MAPbI_3$ perovskite films [31].

To clarify how SnO_2/F–ZnO affected the crystal development of the perovskite layer, the morphologies and compositional characterizations of the perovskite films fabricated on different ETLs (i.e., untreated or treated SnO_2 layers with 3.0%, 6.0%, and 9.0% F–ZnO solutions) are investigated (Fig. 3). It has already been reported that the substrates impacted the perovskite film's structure [32] (Cite this paper also: https://doi.org/10.1007/s40820-022-00992-5).

For two reasons, a perovskite with passivated grain boundaries (GBs) is preferred. First, grain boundaries will act as charge recombination centers. Therefore, the passivated GBs offer lower the density of charge traps per volume, suppressing the troublesome charge recombination

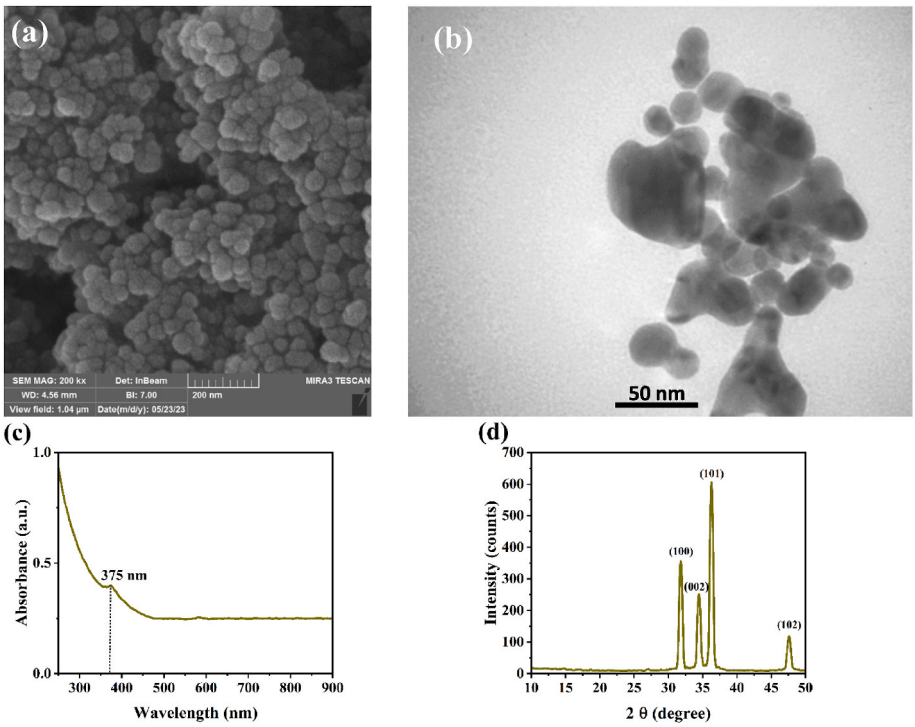

Fig. 1. Characterization of synthesized fluorine doped-zinc oxide nanoparticles. (a) FESEM, (b) TEM, (c) UV–Vis, and (d) XRD pattern.

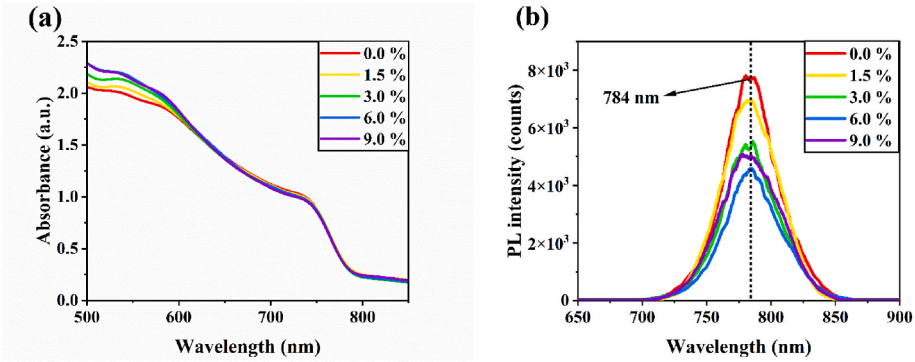

Fig. 2. (a) Absorbance and (b) PL spectra of different perovskite layers. To measure absorbance and PL, perovskite layers were deposited on untreated and treated SnO_2 layers.

and increasing the solar cell's Voc and FF [33,34]. Second, the passivated GBs in perovskite are more likely to allow photoinduced charges to move over extended distances during the charge transfer process, which can enhance the device's performance [35,36]. Fig. 3a–d displays top-view FESEM images of different perovskites. Fig. 3a shows that the untreated film has some pinholes and voids near its obvious GBs, while Fig. 3c shows that the perovskite produced on the SnO_2 ETL treated with the 6.0% F–ZnO solution has a compact coverage of the substrate with considerably met grains without any voids. In addition, the perovskite crystal on SnO_2 modified with the 6.0% F–ZnO solution became more homogeneous than pure SnO_2. It shows that SnO_2 modified with a 6.0% F–ZnO solution can optimize the perovskite morphologies, which is advantageous for light absorption and charge transport. A homogenous perovskite layer with good surface coverage is ideal for high-performance solar cells since pinholes could result in direct contact between the ETL and the HTL or electrode, creating a shunting channel. Notably, as shown in Fig. 3d, by increasing the concentration of F–ZnO solution for the treatment of the SnO_2 layer, the fabricated perovskite layer shows undesirable morphologies. The grains, in this case, push each other and lead to vertical perovskite growth, and bring us a wrinkled perovskite film.

Fig. 4a illustrates the X-ray diffraction (XRD) patterns used to assess the impact of the F–ZnO treatment on the final perovskite crystallinity. The perovskite crystal's development orientation on the SnO_2 films was unaffected by the 6% F–ZnO, and all of the peaks in the XRD patterns could be correlated to the tetragonal crystal structure of $MAPbI_3$ [37]. It was also discovered that when the perovskite films grew on the 6% F–ZnO treated SnO_2 substrates, these perovskite diffraction peaks significantly strengthened, indicating improved crystallinity of perovskite films [38]. These findings and the FESEM measurements (Fig. 3) are in good agreement. Additionally, the perovskite layer made on the untreated SnO_2 film has an X-ray peak at $2\Theta = 12.6^\circ$ (PbI_2 phase), indicating an incomplete reaction of MAI with PbI_2 (See Fig. 4b). The perovskite layer made on modified SnO_2 with 6% F–ZnO solution had a weaker PbI_2 peak intensity, confirming the modified $SnO_2/MAPbI_3$ interface has benefits to form a favored $MAPbI_3$ with better light-harvesting ability.

We first investigate how the F–ZnO proportion affects photovoltaic

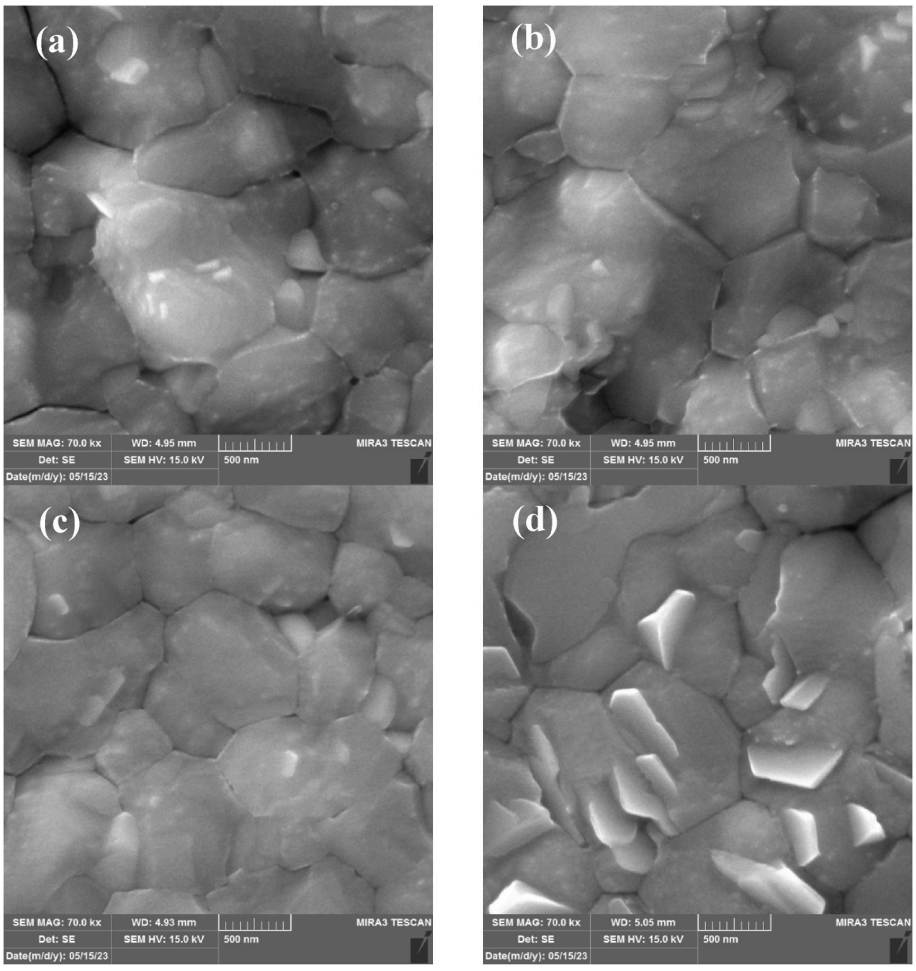

Fig. 3. FESEM image of fabricated perovskite layer on the (a) untreated and treated SnO_2 layer with (b) 3.0%, (c) 6.0%, and (d) 9.0% F–ZnO solution.

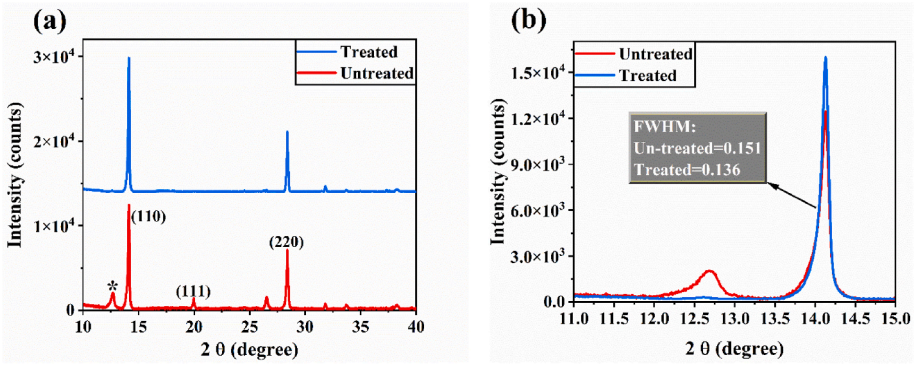

Fig. 4. (a) XRD pattern of perovskite layers fabricated on untreated and treated SnO_2 with 6% F–ZnO solution. (b) Zoomed-view XRD pattern around $2\Theta = 13$ °.

performance (Fig. 5a). Table 1 lists the average and maximum photovoltaic parameters, and Fig. 5b displays statistical photovoltaic performance based on different F–ZnO solution concentrations. It is clear from observation that F–ZnO 6% yields the maximum power conversion efficiency (PCE). The following data are based on SnO_2, which has been modified with F–ZnO 6%. As a result of the modification, the average short-circuit current density (J_{SC}) increased marginally from 19.86 mA cm^{-2} to 20.14 mA cm^{-2}, which is attributed to a minor improvement in absorbance (Fig. 2a) and charge collection ability (Fig. 2b). In addition, a decrease in interfacial charge transfer resistance may cause an increase in the average fill factor (FF) from 62.75 to 73.64%. The average PCE of the untreated device thus increases from 11.33% to 14.72%, mainly as a result of a significantly increased average open-circuit voltage (V_{OC}) from 908 mV to 992 mV, which is linked to decreased charge recombination and efficient defect passivation.

The dark current density-voltage (J-V) of carbon-based HTL-free PSCs fabricated on the untreated and treated SnO_2 layers was measured to find reasons for the enhanced performance of treated solar cells (Fig. 6a). J-V curves demonstrate that the leakage current of the device with a treated SnO_2 layer is lower than the device with an untreated SnO_2 layer. It suggests that device flaws cause leakage current, and since the solar cells fabricated on the treated SnO_2 layer have fewer defect

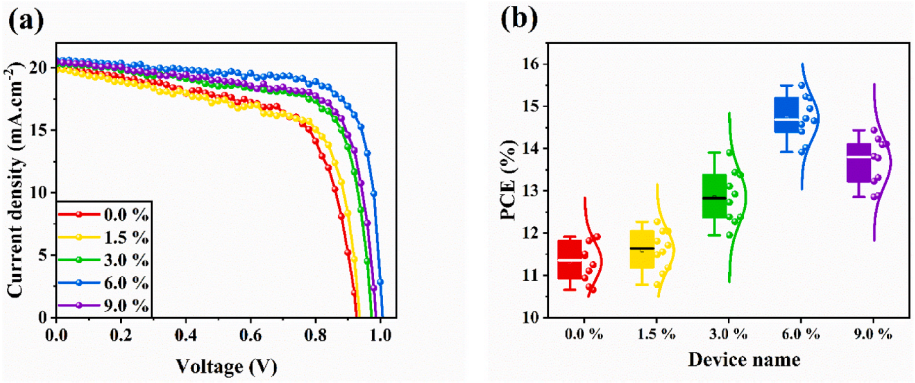

Fig. 5. (a) J-V curves of champion carbon-based HTL-free PSCs fabricated on different SnO_2 layers. (b) Statistics distribution of PCE measured from 10 solar cells in each group.

Table 1
Photovoltaic parameters of carbon-based HTL-free PSCs fabricated on treated SnO_2 layers with F–ZnO solution with different concentrations.

F–ZnO solution concentration		V_{oc} (mV)	J_{sc} (mA/cm^2)	FF (%)	PCE (%)
0.0%	Average	908	19.86	62.75	11.33
	Maximum	930	19.93	64.07	11.88
1.5%	Average	920	19.86	63.43	11.59
	Maximum	930	19.81	66.58	12.27
3.0%	Average	958	19.92	67.28	12.85
	Maximum	970	20.30	70.61	13.90
6.0%	Average	992	20.14	73.64	14.72
	Maximum	1010	20.61	74.16	15.50
9.0%	Average	952	20.04	71.66	13.67
	Maximum	970	20.47	71.22	14.43

states, a higher V_{OC} is achieved. In addition, as shown in Fig. 6a, the treated carbon-based HTL-free PSCs have a lower reverse saturation current density (J_0) compared to the untreated device, indicating lower nonradiative recombination in the perovskite layer [39]. By figuring out the relationship between the photoelectric response and incident light intensity, comprehending the recombination mechanism of devices is possible. It can be calculated by plotting J_{SC} as a function of incident light intensity in line with the equation of $Jsc \propto I\alpha$ ($\alpha \leq 1$) [40,41]. In the equation, I denotes the intensity of the light, and α denotes the charge extraction-related cells' exponential factor. The value of α gets closer to 1 as bimolecular recombination is minimized (α ≈ 1). According to the fitted data in Fig. 6b, the value of α in the SnO_2 and SnO_2/F–ZnO (6%) layers were measured to 0.905 and 0.923, indicating lower bimolecular recombination rate in the treated device, as supported by PL spectra [42,43].

As shown in Fig. 7, the stability of the carbon-based HTL-free PSCs was tested in ambient air with a humidity of roughly 30% in the dark at RT. The treated device exhibits exceptional stability after 2100 h of continuous testing, maintaining 96% of its initial PCE, as opposed to 89% for the untreated device under the same circumstances. Contrary to the $MAPbI_3$ film on bare SnO_2 substrate, the $MAPbI_3$ film on SnO_2-6.0% F–ZnO exhibits homogeneous morphology with passivated GBs and a greater water contact angle. The treated SnO_2 layers raised the contact angle value from 58.4° to 74.2°, as illustrated in the inset of Fig. 7. According to the findings mentioned above, F–ZnO can help perovskite grow to a desirable morphology, shielding the perovskite coating from moisture and water damage to improve device stability.

3. Conclusion

The obtained results show that SnO_2 treated with F–ZnO solution (6%) as ETL will effectively improve the performance of carbon-based HTL-free PSCs. The F–ZnO treatment helps photovoltaic devices with interface passivation and lowers charge recombination. The treated SnO_2/perovskite interface had achieved remarkable success in lowering the defect density in the perovskite layer, thereby increasing the efficiency of electron transport from the perovskite layer to the ETL. With an actual improvement in the FF, the treated carbon-based HTL-free PSCs showed the best PCE performance of 15.50%, higher than the efficiency of 11.88% recorded for untreated devices. After 2100 h in an environment with a humidity of about 30% in the dark at RT, the unencapsulated optimized device retains 96% of its initial efficiency. In contrast, in the same condition, the untreated device maintains 89% of its initial efficiency. This simple approach to the tin oxide ETL could offer a straightforward method to create carbon-based perovskite photovoltaics with appreciable performance gains.

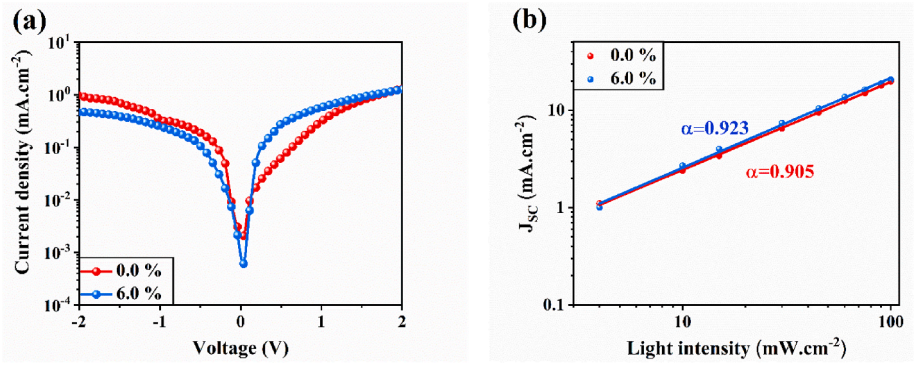

Fig. 6. (a) Dark current density-voltage of carbon-based HTL-free PSCs fabricated on the untreated SnO_2 (0.0%) and treated SnO_2 with F–ZnO solution (6.0%). (b) Curves of J_{SC} versus light intensity for the untreated and treated SnO_2-based carbon-based HTL-free PSCs. α indicates the ideality factor of a solar cell.

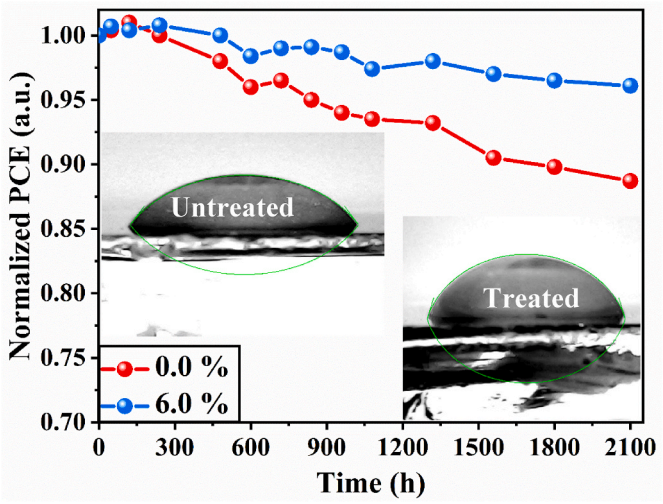

Fig. 7. Stability test of un-sealed carbon-based H TL-free PSCs fabricated based on untreated (0.0%) and treated (6.0%) SnO_2 ET Ls. The inset image shows contact angle water droplets on the perovskite layer fabricated on the untreated and treated SnO_2 layers.

Availability of data and materials

Data will be available based on reasonable request.

CRediT authorship contribution statement

Anupam Yadav: Conceptualization, Writing – original draft. **M.I. Sayyed:** Writing – review & editing. **Nafis Ahmad:** Writing – original draft, and, Formal analysis. **S. Kevin Vargas-Portugal:** Language correction. **A.M. Alshehri:** Experimentation. **Anmar Ghanim Taki:** Experimentation. **Russul thabit:** Result, Formal analysis, and, Validation. **Ayat Hussein Adhab:** Supervision, and editing.

Declaration of competing interest

The authors declare no competing financial interest.

Data availability

Data will be made available on request.

Acknowledgements

The authors extend their appreciation to the Deanship of Scientific Research at King Khalid University for funding this work through the large group Research Project under grant number RGP 2/247/44.

References

[1] A. Kumar, S. Singh, M. Al-Bahrani, Enhancement in power conversion efficiency and stability of perovskite solar cell by reducing trap states using trichloroacetic acid additive in anti-solvent, Surface. Interfac. 34 (2022), 102341.
[2] M. Dehghanipour, A. Behjat, A. Shabani, M. Haddad, Toward desirable 2D/3D hybrid perovskite films for solar cell application with additive engineering approach, J. Mater. Sci. Mater. Electron. (2022) 1–12.
[3] N. Torabi, A. Behjat, Y. Zhou, P. Docampo, R.J. Stoddard, H.W. Hillhouse, T. Ameri, Progress and challenges in perovskite photovoltaics from single-to multi-junction cells, Mater. Today Energy 12 (2019) 70–94.
[4] A. Kumar, M. Sayyed, M.M. Sabugaa, R. Seemaladinne, J.C.O. Gavilán, P. Singh, A. Sharma, T.C.A. Kumar, Potassium hexacyanoferrate (III): a promising additive for perovskite precursors in carbon-based perovskite solar cells, Opt. Mater. 142 (2023), 113986.
[5] S. Wang, P. Wang, B. Chen, R. Li, N. Ren, Y. Li, B. Shi, Q. Huang, Y. Zhao, M. Grätzel, Suppressed Recombination for Monolithic Inorganic Perovskite/silicon Tandem Solar Cells with an Approximate Efficiency of 23%, eScience, 2022.
[6] D.A. Noori, A. Behjat, M. Dehghanipour, Operational stability study of hole transport-free perovskite solar cells using lithium fluoride in electron transport layer, J. Mater. Sci. Mater. Electron. 34 (7) (2023) 592.
[7] Z. Zhang, M.A. Kamarudin, A.K. Baranwal, G. Kapil, S.R. Sahamir, Y. Sanehira, M. Chen, L. Wang, Q. Shen, S. Hayase, Sequential passivation for lead-free tin perovskite solar cells with high efficiency, Angew. Chem. (2022).
[8] G. Nagaraj, M.K.A. Mohammed, M. Shekargoftar, P. Sasikumar, P. Sakthivel, G. Ravi, M. Dehghanipour, S. Akin, A.E. Shalan, High-performance perovskite solar cells using the graphene quantum dot–modified SnO2/ZnO photoelectrode, Mater. Today Energy 22 (2021), 100853.
[9] A. Kojima, K. Teshima, Y. Shirai, T. Miyasaka, Organometal halide perovskites as visible-light sensitizers for photovoltaic cells, J. Am. Chem. Soc. 131 (17) (2009) 6050–6051.
[10] A. Kumar, M. Sayyed, M.M. Sabugaa, S. Singh, J.C.O. Gavilán, A. Sharma, Additive engineering with sodium azide material for efficient carbon-based perovskite solar cells, New J. Chem. 47 (16) (2023) 7765–7773.
[11] H. Min, D.Y. Lee, J. Kim, G. Kim, K.S. Lee, J. Kim, M.J. Paik, Y.K. Kim, K.S. Kim, M. G. Kim, Perovskite solar cells with atomically coherent interlayers on SnO2 electrodes, Nature 598 (7881) (2021) 444–450.
[12] S.H. Kareem, M.H. Elewi, A.M. Naji, D.S. Ahmed, M.K. Mohammed, Efficient and stable pure α-phase FAPbI3 perovskite solar cells with a dual engineering strategy: additive and dimensional engineering approaches, Chem. Eng. J. 443 (2022), 136469.
[13] M.K.A. Mohammed, M. Dehghanipour, U. Younis, A.E. Shalan, P. Sakthivel, G. Ravi, P.H. Bhoite, J. Pospisil, Improvement of the interfacial contact between zinc oxide and a mixed cation perovskite using carbon nanotubes for ambient-air-processed perovskite solar cells, New J. Chem. 44 (45) (2020) 19802–19811.
[14] A. Kumar, S. Singh, M.K. Mohammed, D.S. Ahmed, Experimental investigation of additive free-low-cost vinyl triarylamines based hole transport material for FAPbI3-based perovskite solar cells to enhance efficiency and stability, Mater. Res. Express 10 (4) (2023), 044003.
[15] J.Y. Seo, S. Akin, M. Zalibera, M.A.R. Preciado, H.S. Kim, S.M. Zakeeruddin, J. V. Milić, M. Grätzel, Dopant engineering for SPIRO-OMeTAD hole-transporting materials towards efficient perovskite solar cells, Adv. Funct. Mater. 31 (45) (2021), 2102124.
[16] T. Niu, W. Zhu, Y. Zhang, Q. Xue, X. Jiao, Z. Wang, Y.-M. Xie, P. Li, R. Chen, F. Huang, DA-π-AD-type dopant-free hole transport material for low-cost, efficient, and stable perovskite solar cells, Joule 5 (1) (2021) 249–269.
[17] F.M. Rombach, S.A. Haque, T.J. Macdonald, Lessons Learned from Spiro-OMeTAD and PTAA in Perovskite Solar Cells, Energy & Environmental Science, 2021.
[18] M. Batmunkh, C.J. Shearer, M.J. Biggs, J.G. Shapter, Nanocarbons for mesoscopic perovskite solar cells, J. Mater. Chem. A 3 (17) (2015) 9020–9031.
[19] H. Zhang, J. Xiao, J. Shi, H. Su, Y. Luo, D. Li, H. Wu, Y.B. Cheng, Q. Meng, Self-adhesive macroporous carbon electrodes for efficient and stable perovskite solar cells, Adv. Funct. Mater. 28 (39) (2018), 1802985.
[20] L. Fagiolari, F. Bella, Carbon-based materials for stable, cheaper and large-scale processable perovskite solar cells, Energy Environ. Sci. 12 (12) (2019) 3437–3472.
[21] A. Kumar, S. Singh, A. Sharma, E.M. Ahmed, Efficient and stable perovskite solar cells by interface engineering at the interface of electron transport layer/perovskite, Opt. Mater. 132 (2022), 112846.
[22] H. Chen, Z. Wei, H. He, X. Zheng, K.S. Wong, S. Yang, Solvent engineering boosts the efficiency of paintable carbon-based perovskite solar cells to beyond 14, Adv. Energy Mater. 6 (8) (2016), 1502087.
[23] L. Zhou, Y. Zuo, T.K. Mallick, S. Sundaram, Enhanced efficiency of carbon-based mesoscopic perovskite solar cells through a tungsten oxide nanoparticle additive in the carbon electrode, Sci. Rep. 9 (1) (2019) 1–8.
[24] M. Omrani, R. Keshavarzi, M. Abdi-Jalebi, P. Gao, Impacts of plasmonic nanoparticles incorporation and interface energy alignment for highly efficient carbon-based perovskite solar cells, Sci. Rep. 12 (1) (2022) 5367.
[25] R.M. Youssef, A. Salem, A. Shawky, S. Ebrahim, M. Soliman, M.S. Abdel-Mottaleb, S.M. El-Sheikh, Solution-processed quantum dot SnO2 as an interfacial electron transporter for stable fully-air-fabricated metal-free perovskite solar cells, Journal of Materiomics 8 (6) (2022) 1172–1183.
[26] X. Qiu, Y. Xu, R. Li, Y. Jing, Z. Yan, F. Liu, L. Wu, Y. Tu, J. Shi, Z. Du, High-efficiency carbon-based CsPbI2Br perovskite solar cells from dual direction thermal diffusion treatment with cadmium halides, Small (2023), 2206245.
[27] Z. Shi, S. Li, C. Min, J. Xie, R. Ma, Modification of energy levels by cetyltrimethylammonium bromide at the perovskite/carbon interface for highly efficient and stable perovskite solar cells, Org. Electron. 112 (2023), 106689.
[28] T. Zhong, K. Tang, W. Xu, L. Shi, J. Dong, H. Liu, J. Xing, H. Hao, NH4Ac boosts the efficiency of carbon-based all-inorganic perovskite solar cells fabricated in the full ambient air to 15.43, Appl. Surf. Sci. 610 (2023), 155175.
[29] M. Pudukudy, Z. Yaakob, Facile synthesis of quasi spherical ZnO nanoparticles with excellent photocatalytic activity, J. Cluster Sci. 26 (2015) 1187–1201.
[30] S.D. Lee, S.-H. Nam, M.-H. Kim, J.-H. Boo, Synthesis and photocatalytic property of ZnO nanoparticles prepared by spray-pyrolysis method, Phys. Procedia 32 (2012) 320–326.
[31] H.R. Mohseni, M. Dehghanipour, N. Dehghan, F. Tamaddon, M. Ahmadi, M. Sabet, A. Behjat, Enhancement of the photovoltaic performance and the stability of perovskite solar cells via the modification of electron transport layers with reduced graphene oxide/polyaniline composite, Sol. Energy 213 (2021) 59–66.
[32] Q. Lin, A. Armin, R.C.R. Nagiri, P.L. Burn, P. Meredith, Electro-optics of perovskite solar cells, Nat. Photonics 9 (2) (2015) 106–112.
[33] D. Shi, V. Adinolfi, R. Comin, M. Yuan, E. Alarousu, A. Buin, Y. Chen, S. Hoogland, A. Rothenberger, K. Katsiev, Low trap-state density and long carrier diffusion in

organolead trihalide perovskite single crystals, Science 347 (6221) (2015) 519–522.
[34] N.-G. Park, Crystal growth engineering for high efficiency perovskite solar cells, CrystEngComm 18 (32) (2016) 5977–5985.
[35] M. Dehghanipour, A. Behjat, H.A. Bioki, Fabrication of stable and efficient 2D/3D perovskite solar cells through post-treatment with TBABF 4, J. Mater. Chem. C 9 (3) (2021) 957–966.
[36] T. Niu, J. Lu, R. Munir, J. Li, D. Barrit, X. Zhang, H. Hu, Z. Yang, A. Amassian, K. Zhao, Stable high-performance perovskite solar cells via grain boundary passivation, Adv. Mater. 30 (16) (2018), 1706576.
[37] E. Smecca, Y. Numata, I. Deretzis, G. Pellegrino, S. Boninelli, T. Miyasaka, A. La Magna, A. Alberti, Stability of solution-processed MAPbI 3 and FAPbI 3 layers, Phys. Chem. Chem. Phys. 18 (19) (2016) 13413–13422.
[38] G. Yang, C. Wang, H. Lei, X. Zheng, P. Qin, L. Xiong, X. Zhao, Y. Yan, G. Fang, Interface engineering in planar perovskite solar cells: energy level alignment, perovskite morphology control and high performance achievement, J. Mater. Chem. A 5 (4) (2017) 1658–1666.
[39] M.K.A. Mohammed, A.E. Shalan, M. Dehghanipour, H.R. Mohseni, Improved mixed-dimensional 3D/2D perovskite layer with formamidinium bromide salt for highly efficient and stable perovskite solar cells, Chem. Eng. J. 428 (2022), 131185.
[40] F. Cai, J. Cai, L. Yang, W. Li, R.S. Gurney, H. Yi, A. Iraqi, D. Liu, T. Wang, Molecular engineering of conjugated polymers for efficient hole transport and defect passivation in perovskite solar cells, Nano Energy 45 (2018) 28–36.
[41] K. Lu, Y. Wang, J. Yuan, Z. Cui, G. Shi, S. Shi, L. Han, S. Chen, Y. Zhang, X. Ling, Efficient PbS quantum dot solar cells employing a conventional structure, J. Mater. Chem. A 5 (45) (2017) 23960–23966.
[42] M. Jeong, I.W. Choi, E.M. Go, Y. Cho, M. Kim, B. Lee, S. Jeong, Y. Jo, H.W. Choi, J. Lee, Stable perovskite solar cells with efficiency exceeding 24.8% and 0.3-V voltage loss, Science 369 (6511) (2020) 1615–1620.
[43] B.-w. Park, H.W. Kwon, Y. Lee, D.Y. Lee, M.G. Kim, G. Kim, K.-j. Kim, Y.K. Kim, J. Im, T.J. Shin, Stabilization of formamidinium lead triiodide α-phase with isopropylammonium chloride for perovskite solar cells, Nat. Energy 6 (4) (2021) 419–428.